Am J Physiol Gastrointest Liver Physiol 317: G694–G706, 2019.
First published September 11, 2019; doi:10.1152/ajpgi.00116.2019.

RESEARCH ARTICLE | *Brain-Gut Interactions*

Human pancreatic afferent and efferent nerves: mapping and 3-D illustration of exocrine, endocrine, and adipose innervation

Hung-Jen Chien,[1]* Tsai-Chen Chiang,[2]* Shih-Jung Peng,[1,3] Mei-Hsin Chung,[1,4] Ya-Hsien Chou,[1,3] Chih-Yuan Lee,[2] Yung-Ming Jeng,[5] Yu-Wen Tien,[2]* and Shiue-Cheng Tang[1,3]*

[1]*Institute of Biotechnology, National Tsing Hua University, Hsinchu, Taiwan;* [2]*Department of Surgery, National Taiwan University Hospital, Taipei, Taiwan;* [3]*Department of Medical Science, National Tsing Hua University, Hsinchu, Taiwan;* [4]*Department of Pathology, National Taiwan University Hospital-Hsinchu Branch, Hsinchu, Taiwan; and* [5]*Department of Pathology, National Taiwan University Hospital, Taipei, Taiwan*

Submitted 2 May 2019; accepted in final form 3 September 2019

Chien HJ, Chiang TC, Peng SJ, Chung MH, Chou YH, Lee CY, Jeng YM, Tien YW, Tang SC. Human pancreatic afferent and efferent nerves: mapping and 3-D illustration of exocrine, endocrine, and adipose innervation. *Am J Physiol Gastrointest Liver Physiol* 317: G694–G706, 2019. First published September 11, 2019; doi:10.1152/ajpgi.00116.2019.—The pancreas consists of both the exocrine (acini and ducts) and endocrine (islets) compartments to participate in and regulate the body's digestive and metabolic activities. These activities are subjected to neural modulation, but characterization of the human pancreatic afferent and efferent nerves remains difficult because of the lack of three-dimensional (3-D) image data. Here we prepare transparent human donor pancreases for 3-D histology to reveal the pancreatic microstructure, vasculature, and innervation in a global and integrated fashion. The pancreatic neural network consists of the substance P (SP)-positive sensory (afferent) nerves, the vesicular acetylcholine transporter (VAChT)-positive parasympathetic (efferent) nerves, and the tyrosine hydroxylase (TH)-positive sympathetic (efferent) nerves. The SP^+ afferent nerves were found residing along the basal domain of the interlobular ducts. The $VAChT^+$ and TH^+ efferent nerves were identified at the peri-acinar and perivascular spaces, which follow the blood vessels to the islets. In the intrapancreatic ganglia, the SP^+ (scattered minority, ~7%) and $VAChT^+$ neurons co-localize, suggesting a local afferent-efferent interaction. Compared with the mouse pancreas, the human pancreas differs in *1*) the lack of SP^+ afferent nerves in the islet, *2*) the lower ganglionic density, and *3*) the obvious presence of $VAChT^+$ and TH^+ nerves around the intralobular adipocytes. The latter implicates the neural influence on the pancreatic steatosis. Overall, our 3-D image data reveal the human pancreatic afferent and efferent innervation patterns and provide the anatomical foundation for future high-definition analyses of neural remodeling in human pancreatic diseases.

NEW & NOTEWORTHY Modern three-dimensional (3-D) histology with multiplex optical signals identifies the afferent and efferent innervation patterns of human pancreas, which otherwise cannot be defined with standard histology. Our 3-D image data reveal the unexpected association of sensory and parasympathetic nerves/neurons in the intrapancreatic ganglia and identify the sympathetic and parasympathetic nerve contacts with the infiltrated adipocytes. The multiplex approach offers a new way to characterize the human pancreas in remodeling (e.g., fatty infiltration and duct lesion progression).

autonomic innervation; fatty infiltration; intrapancreatic ganglia; pancreatic steatosis; tissue clearing

INTRODUCTION

The human pancreas is an exocrine organ with acini and ducts as the functional subunits to secrete and transport digestive enzymes to the proximal duodenum for food digestion. The pancreatic lobules also contain scattered endocrine tissues, the islets, which secrete hormones including glucagon, insulin (accompanied with amylin), somatostatin, ghrelin, and pancreatic polypeptide from α-, β-, δ-, ε-, and γ-cells, respectively, to modulate metabolic activities and to maintain energy (glucose) homeostasis. Studies of human and animal pancreases indicate that both the enzyme and hormone secretions are under neural control in response to physiological cues (1, 4, 32, 59). For example, in meal anticipation and ingestion, the cephalic responses of islet hormone secretion [e.g., insulin, amylin, glucagon, and pancreatic polypeptide secretion (27, 42, 57)] have been attributed to autonomic activation (1, 2, 8, 58). Meanwhile, in the action of vago-vagal reflex, the mechanical and chemical stimulations from foods in the upper gastrointestinal tract generate sensory (afferent) nerve inputs to the dorsal vagal complex, in which motor outputs are created and travel back to the pancreas and intestine via the efferent parasympathetic nerves, stimulating both organs for continuous production and influx of enzymes to the duodenum (37). Conversely, in the critical condition of severe hypoglycemia, the activation of sympathetic nerves (efferent) contributes to the increase in glucagon secretion and the suppression of insulin secretion from the islet α- and β-cells, respectively, to restore euglycemia (1, 52).

In pancreatic diseases, the injuries and remodeling of pancreatic microstructures are often associated with changes in the neural structure and/or activity. For example, pain is a hallmark symptom in pancreatitis and pancreatic cancer (11, 13). The symptom indicates the activation of afferent sensory nerves. However, their innervation patterns in the human pancreas have been largely unknown. Regarding the efferent nerves, the loss of islet sympathetic nerves has been observed in experimental type 1 diabetes [nonobese diabetic mice (51) and biobreeding rats (36)] and is proposed in patients with diabetes. The islet neuropathy, in addition to other defective mecha-

* H.-J. Chien and T.-C. Chiang contributed equally to this work. Y.-W. Tien and S.-C. Tang contributed equally to this work.

Address for reprint requests and other correspondence: S.-C. Tang, National Tsing Hua University, 101, Sec. 2, Kuang Fu Rd., Hsinchu, Taiwan 30013 (e-mail: sctang@life.nthu.edu.tw).

nisms in type 1 diabetes (e.g., loss of intra-islet β-cell/GABA-mediated disinhibition of α-cells) (34, 52, 63), could partly account for the loss of glucagon counter-response to the insulin-induced hypoglycemia in patients who receive intensive insulin therapy.

Despite the important roles of pancreatic innervation, prior studies of this field primarily focus on the animals (e.g., rodents) and experimental conditions (1, 5, 9, 32, 49). Identification and illustration of the human pancreatic afferent and efferent nerves are difficult, which is in part due to the technical challenges in acquiring and preparing pancreatic specimens (22). First, as an organ, the pancreas is filled with strong digestive enzymes, which discourage biopsies taken from the healthy or diabetic individuals because of safety concerns. Second, the surgical biopsies acquired from patients with pancreatitis or pancreatic cancer are largely deformed (e.g., acinar atrophy), which cannot reflect the normal pancreatic innervation. Third, the resected pancreas often contains residual blood and quickly undergoes autolysis: the former creates a false positive (autofluorescence) in fluorescent labeling, whereas the latter causes a false negative in signal detection. These difficulties, unfortunately, cause uncertainty in neurohistology and likely contribute to the mixed results about the presence and pattern of human pancreatic exocrine and endocrine innervation (21, 41, 50, 55).

To overcome the challenges in pancreatic neurohistology, previously we prepared transparent donor pancreases for three-dimensional (3-D) imaging and used the pan-neuronal markers to visualize the pancreatic neuro-insular network (55). In this study, we use the 3-D approach to examine the overall pancreatic community (exocrine, endocrine, and ectopic fats) and immunolabel the human pancreases with the classic sensory, parasympathetic, and sympathetic markers to resolve and illustrate the afferent and efferent innervation patterns with multidimensional and multiplex signals. Specifically, the signals include *1*) the transmitted light and fluorescence signals, which detect and confirm the intrinsic (acini, islets, and ducts) and extrinsic (intralobular adipocytes) pancreatic components, and *2*) the tile-scanned and in-depth 3-D signals of pancreatic microstructures, vasculature, and innervation, which identify the intrapancreatic ganglia and depict the innervation patterns in a global and an integrated fashion (55, 56). In addition, we compare the human and mouse pancreatic innervation patterns to highlight the similarities and differences between the two systems. The physiological implications of the adipose innervation and the unexpected association of the sensory and parasympathetic nerves in the human pancreas are discussed.

MATERIALS AND METHODS

Human and mouse pancreatic specimens. Collection and use of human tissues were approved by the Institutional Review Board of National Taiwan University Hospital. Normal human pancreases were obtained from cadaveric organ donors. Perfused pancreases from 4 donors [sex/age (yr)/body mass index: female/40/24, male/53/28, female/51/20, and female/26/22] with normal hemoglobin A_{1c}, amylase, and lipase levels were used to characterize the pancreatic innervation. Additionally, 3 biopsies with duct lesions were obtained from distal pancreatectomy for treatment of ductal adenocarcinoma [(sex/age (yr)/staging: male/77/T1N0, male/52/T2N0, and male/67/T3N0)] to confirm the pancreatic innervation and intrapancreatic ganglia in a disease condition. Immediately after the operation, the dissected biopsies were perfused with 1,000 mL of saline through the splenic artery, which was cannulated with a 21-French peripheral venous catheter, to remove the residual blood. Afterward, the pancreatic tissues were fixed in 4% formaldehyde for 2 days and then washed in saline for 4 days at 4°C. Specimens were later sectioned to 350 μm in thickness by vibratome and transferred to 0.1% paraformaldehyde for preservation at 4°C (55).

Six mouse pancreases acquired from the wild-type male C57BL/6 (B6) mice at age ~12 wk were used to generate the representative images. To prepare for pancreatic vessel labeling, the animals were given a single intraperitoneal injection of Zoletil (Virbac, Carros cedex, France; 200 μg/g body wt; overdose) and then euthanized via transcardiac saline perfusion (1 mL/1 g body wt). Afterward, the vasculature was perfused with the lectin-Alexa Fluor 488 conjugate (Invitrogen, Carlsbad, CA) and followed by 4% paraformaldehyde perfusion fixation (28). Next, the pancreases were dissected and postfixed in 4% paraformaldehyde solution for 40 min at 15°C. Vibratome sections of the fixed pancreases were then prepared, and the sections were transferred to 0.1% paraformaldehyde for preservation at 4°C. The Institutional Animal Care and Use Committees at National Tsing Hua University approved all procedures with mice.

Pancreatic tissue labeling and imaging. The fixed specimens were immersed in 2% Triton X-100 solution for 2 h at 15°C for permeabilization. Seven different primary antibodies were used in combination to immunolabel the tissues following the protocol outlined below. The antibodies used were rabbit anti-PGP9.5 [neuroendocrine marker (24); ab-108986 and ab-196173, Abcam, Cambridge, MA], mouse anti-CD31 (endothelial marker; MS-353-S1, Thermo Scientific, Fremont, CA), mouse anti-glucagon (ab-10988, Abcam), guinea pig anti-insulin (GTX-27842, GeneTex, Irvine, CA), rat anti-substance P [SP; sensory nerve marker (33, 38), MAB-356, Millipore, Billerica, MA], rabbit anti-vesicular acetylcholine transporter [VAChT, parasympathetic marker (3); 139103, Synaptic Systems, Goettingen, Germany], and rabbit anti-tyrosine hydroxylase [TH, sympathetic marker (16); AB-152, Millipore] antibodies. Before applying the antibodies, tissue sections were rinsed in phosphate-buffered saline (PBS). This was followed by a blocking step, incubating the tissue with the blocking buffer (2% Triton X-100, 10% normal goat serum, and 0.02% sodium azide in PBS). The primary antibody was then diluted in the dilution buffer (1:100, 0.25% Triton X-100, 1% normal goat serum, and 0.02% sodium azide in PBS) to replace the blocking buffer and incubated for 2 days at 15°C. Negative staining controls were prepared by omitting the primary antibody in the buffer.

Alexa Fluor 647, 546, and 488 conjugated secondary antibodies (raised in goat; 1:200, Invitrogen) were used in combination to reveal the immunostained structures. DAPI or SYTO 16 staining was performed to reveal the nuclei. To maximize photon penetration in deep-tissue microscopy, the labeled specimens were transferred to an aqueous tissue-clearing solution with high refractive index (RapiClear 1.52 solution, SunJin Laboratory, Hsinchu, Taiwan) overnight and then immersed in a fresh RapiClear solution for 1 day before being imaged via transmitted light and confocal microscopy (12, 55).

Imaging of the tissue structure was performed with Zeiss LSM 800 confocal microscopes (Carl Zeiss, Jena, Germany) equipped with ×10 Fluar (optical section: 10 μm; *z*-axis increment: 5 μm), ×25 LD Plan-Apochromat (working distance: 570 μm; optical section: 5 μm; *z*-axis increment: 2.5 μm), and ×40 LD C-Apochromat (working distance: 620 μm; optical section: 3 μm; *z*-axis increment: 1.5 μm) lenses. Gross views of pancreatic lobules were acquired under ×10 lenses via tile-scan mode with automatic image stitching. The laser-scanning process was operated under the multitrack scanning mode to sequentially acquire signals, including the transmitted light signals. Fluorescence signals in figures are pseudo-colored. Supplemental Tables S1 and S2 (http://doi.org/10.5281/zenodo.3373231)

summarize the color codes for different markers and the immunostaining reagents/dilutions used in the illustrations, respectively.

Image signal processing, projection, and quantitation. The Avizo 6.2 image reconstruction software (VSG, Burlington, MA), Zen software (Carl Zeiss), and LSM510 software (Carl Zeiss) were used for projection, signal segmentation, noise reduction (Gaussian filter; kernel 3 × 3), and analysis of confocal images. Quantitation of the nerve density was previously illustrated by Juang et al. (23). In the estima-

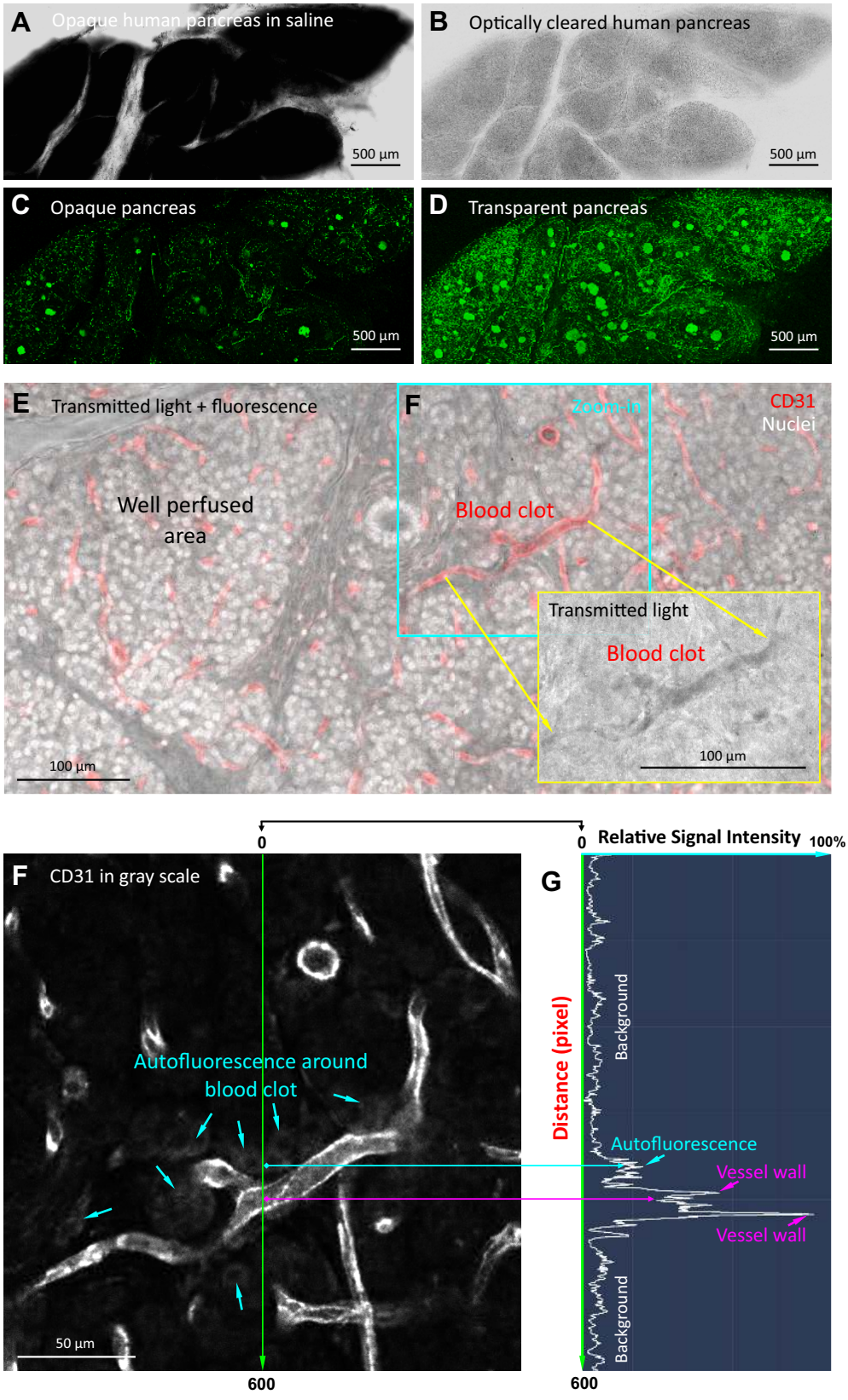

Fig. 1. Deep-tissue microscopy of human pancreas: false-negative and false-positive results. False-negative result due to tissue opacity (*A–D*). Opaque human pancreas (female, age 26 yr, body mass index 22) blocks signals in transmitted light (*A*) and fluorescence (*C*) imaging. Situation is relieved with optical clearing (*B* and *D*). Green: neuroendocrine marker PGP9.5 staining of nerves and islets. Projection depth: 300 µm (*C* and *D*). False-positive result due to residual blood in specimen (*E–G*). *E* shows a blood clot (*inset*, yellow box) in the pancreatic parenchyma after overlaying the fluorescence and transmitted light signals. Red: CD31 staining of endothelium. Gray: nuclear staining. Cyan box is enlarged in *F*. Signal analysis of the green line in *F* (600 pixels) is presented in *G*. Cyan arrows in *F* and *G* indicate the blood clot-induced autofluorescence (3.4 ± 0.8 -fold of background signal intensity; $n = 6$ images; $P < 0.001$; signal segmentation and quantitation were performed using Zeiss Zen 2.1 SP2 software and analyzed with two-tailed Student's *t* test). Magenta arrow in *G*: CD31 signal of vessel wall.

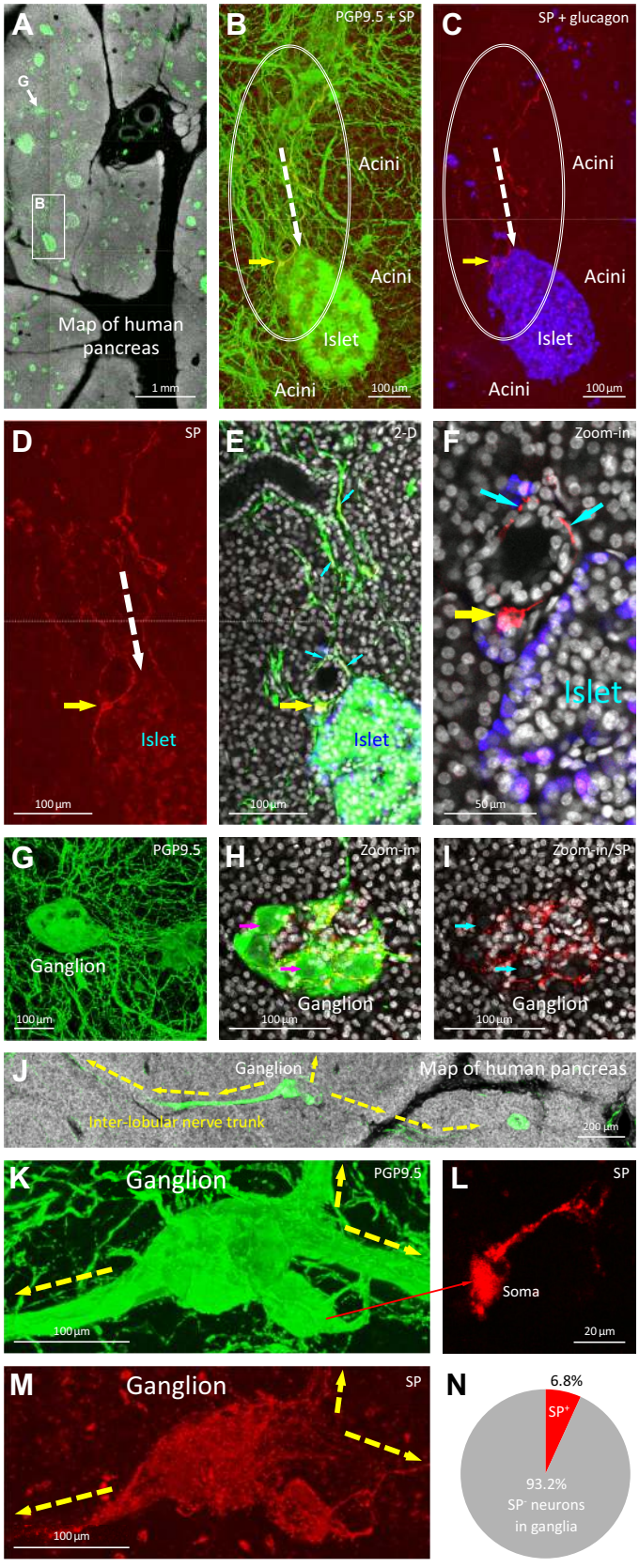

tion, feature extraction and image segmentation were first performed by the Label Field function of Avizo to collect the voxels of islets and the surrounding acini (within ~500 μm) and their associated SP^+ nerve fibers and varicosities but exclude the globular SP^+ cells. Afterward, the voxels of islet (or acinus)-associated nerves were divided by those of the islets (or acini) × 100% to estimate the nerve density. The same immunolabeling, imaging, and quantitation processes were conducted on the comparable pancreatic sections to characterize the nerve density on the same basis.

Statistical analysis. The quantitative values are presented as means ± SD. Statistical differences were determined by the unpaired Student's *t* test. Differences between groups were considered statistically significant when $P < 0.05$.

RESULTS

False negative and false positive in deep-tissue fluorescence imaging of human pancreas. The lobules of the human pancreas are intrinsically opaque (Fig. 1*A*). Thus, in deep-tissue neurohistology, tissue clearing [or optical clearing (15, 30, 31), Fig. 1*B* is essential to facilitate light transmission to avoid signal loss due to scattering (false negative). This step is crucial to both fluorescence and transmitted light microscopy: the former requires fluorescence to emit from the labeled nerves inside the tissue for imaging (Fig. 1, *C* vs. *D*), whereas the latter requires light transmission across the specimen for detection (Fig. 1, *A* vs. *B*). Between the two signal sources, the transmitted light signals serve as the ground-truth information to verify the tissue structure and network revealed via fluorescence imaging (Fig. 1, *B* vs. *D*).

In particular, the transmitted light signals allow us to detect and avoid areas with blood clots in deep-tissue imaging. Figure 1*E* shows a typical clot in the donor pancreas, which has been previously perfused. In the specimen, although most of the parenchyma was blood free, scattered areas with blood clots were inevitably present. These clots were identified via transmitted light microscopy with tissue clearing (*inset* in Fig. 1*E*). Further analysis of the clots shows false-positive signals (more than threefold of the background), or autofluorescence, in the peri-clot area (Fig. 1, *F* and *G*), underlining the spillover interference of the residual blood in fluorescence imaging.

Because of the potential false-negative and false-positive interferences in pancreatic neurohistology, it is crucial to

Fig. 2. Human pancreatic afferent nerves in parenchyma. *A–C*: panoramic and enlarged views of pancreatic afferent nerves. Map of pancreas in *A* [female, age 51 yr, body mass index (BMI) 20] is used to locate *inset B* (*B*) and arrow *G* (*G*) for enlargement to present the SP^+ sensory (afferent) nerves. Symbols: oval, nerves at the acinar-islet boundary; dashed arrow, nerves toward islet mantle; yellow arrow, substance P $(SP)^+$ soma. Markers: nuclei, white; PGP9.5, green; SP, red; glucagon, blue. *D–F*: high-definition images of peri-ductal SP^+ afferent nerves. Yellow arrow: SP^+ soma and processes. Cyan arrows, SP^+ nerve fibers and varicosities. SP^+ afferent nerves appear in yellow in *E* (overlap of red SP and green PGP9.5 signals). Note that a portion of islet cells are SP dim. *G–I*: intrapancreatic ganglion filled with SP^+ varicosities. SP^+ varicosities are identified around the boundary of neurons. Arrows (*H*) indicate the neuronal cell bodies (SP^- somas, *I*). *J–N*: SP^+ interlobular neural network. Map (*J*) and enlarged images (*K–M*) confirm that a subset of neurons and the interlobular nerve fibers are SP^+. *K* and *M*: projections of the ganglion in *J*. Dashed arrows, directions of interlobular nerves. *L*: SP^+ neuron (bottom right of *K*, red arrow). *N*: percentage of SP^+ neurons in intrapancreatic ganglia. Two hundred and six neurons were analyzed in 4 human pancreases (sex/age (yr)/BMI: female/40/24, male/53/28, female/51/20, and female/26/22). 2-D, two-dimensional.

acquire multidimensional (panoramic two-dimensional and in-depth 3-D) and multiplex signals (transmitted light and paired fluorescence signals) to cross-validate the novel innervation patterns as described in the next five sections.

Mapping and 3-D illustration of human pancreatic afferent nerves in parenchyma. The classic neuropeptides to identify the afferent sensory nerves are the calcitonin gene-related peptide (CGRP) and SP (14, 33, 38). In our parallel tests, the

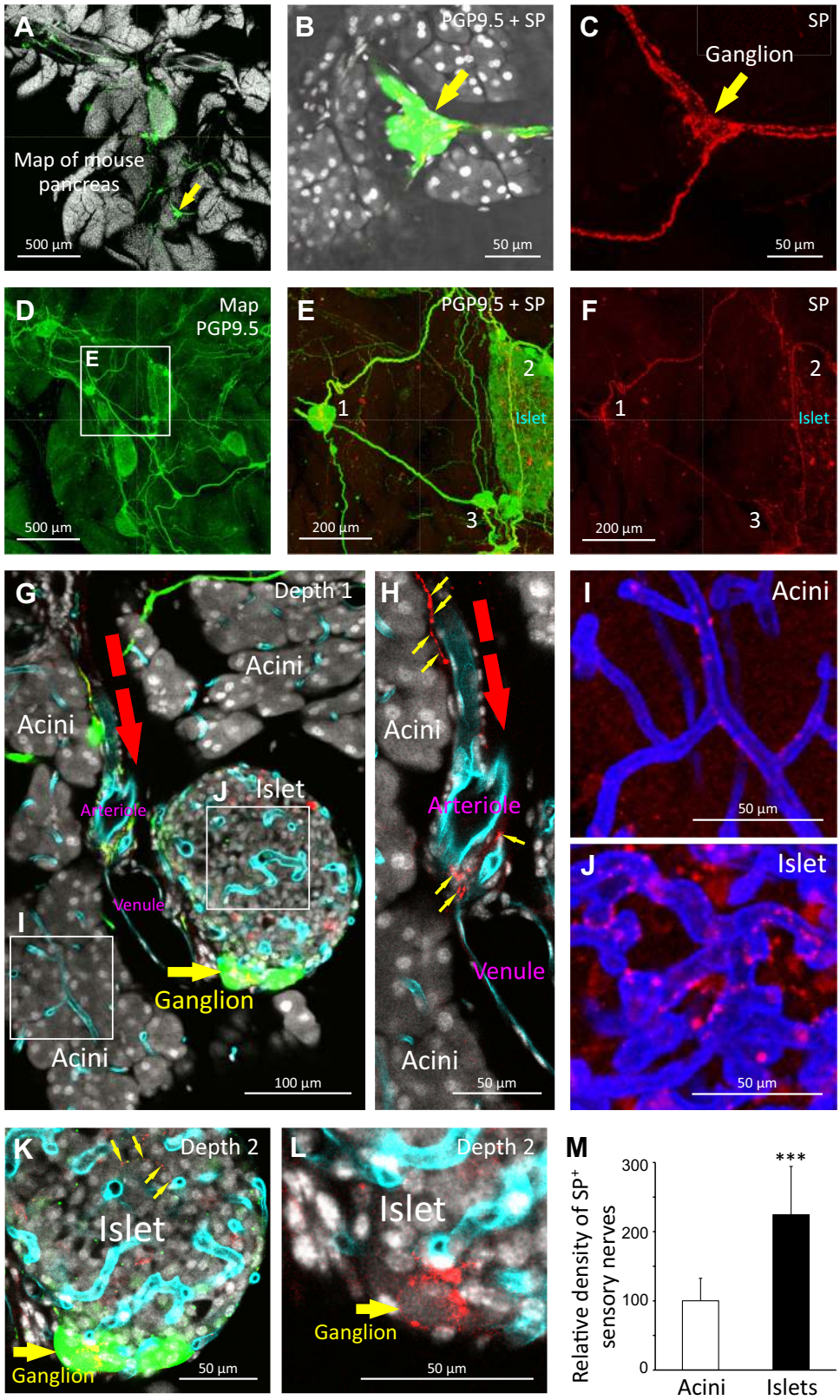

Fig. 3. Characterization of mouse pancreatic afferent nerves. *A–F*: map of mouse pancreas and substance P $(SP)^+$ interlobular neural network. The same region is examined in *A* (two-dimensional image; male, age 12 wk) and *D* (signal projection). *A–C*: arrow indicates an SP^+ intrapancreatic ganglion with interlobular nerve projections (counterpart of the ganglion in Fig. 2, *J–M*). *D–F*: projections highlight the pancreatic neural network and the SP^+ sensory nerves. Numbers 1–3 indicate the ganglia. Note that some mouse islet cells are SP^+, similar to those in the human pancreas. Markers: nuclei, white; PGP9.5, green; SP, red. *G–L*: sensory nerve innervation of acinus and islet. *G*: SP^+ sensory nerves at the acinar-islet boundary (enlarged in *H*). The nerves associate with the acini (*I*) and follow the arteriole (dashed red arrow shown in *G* and *H*) to the islet mantle and core (*J–L*). Yellow arrows, SP^+ ganglion (*G*, *K*, *L*) and nerves (*H*, *K*). *G* and *K*: the same islet but at different focal depths. *H–J*: zoom into different areas in *G*. *L*: SP^+ peri-islet ganglion in *K*. Markers: nuclei, white; PGP9.5, green; SP, red; blue/cyan, blood vessels. *M*: higher density of SP^+ sensory nerves in islets than acini in mice (expressed as % of acini). Twelve islets and the surrounding acini in four mouse pancreases were pooled in quantitation; data are presented as means ± SD and analyzed with two-tailed Student's *t* test (***$P < 0.001$).

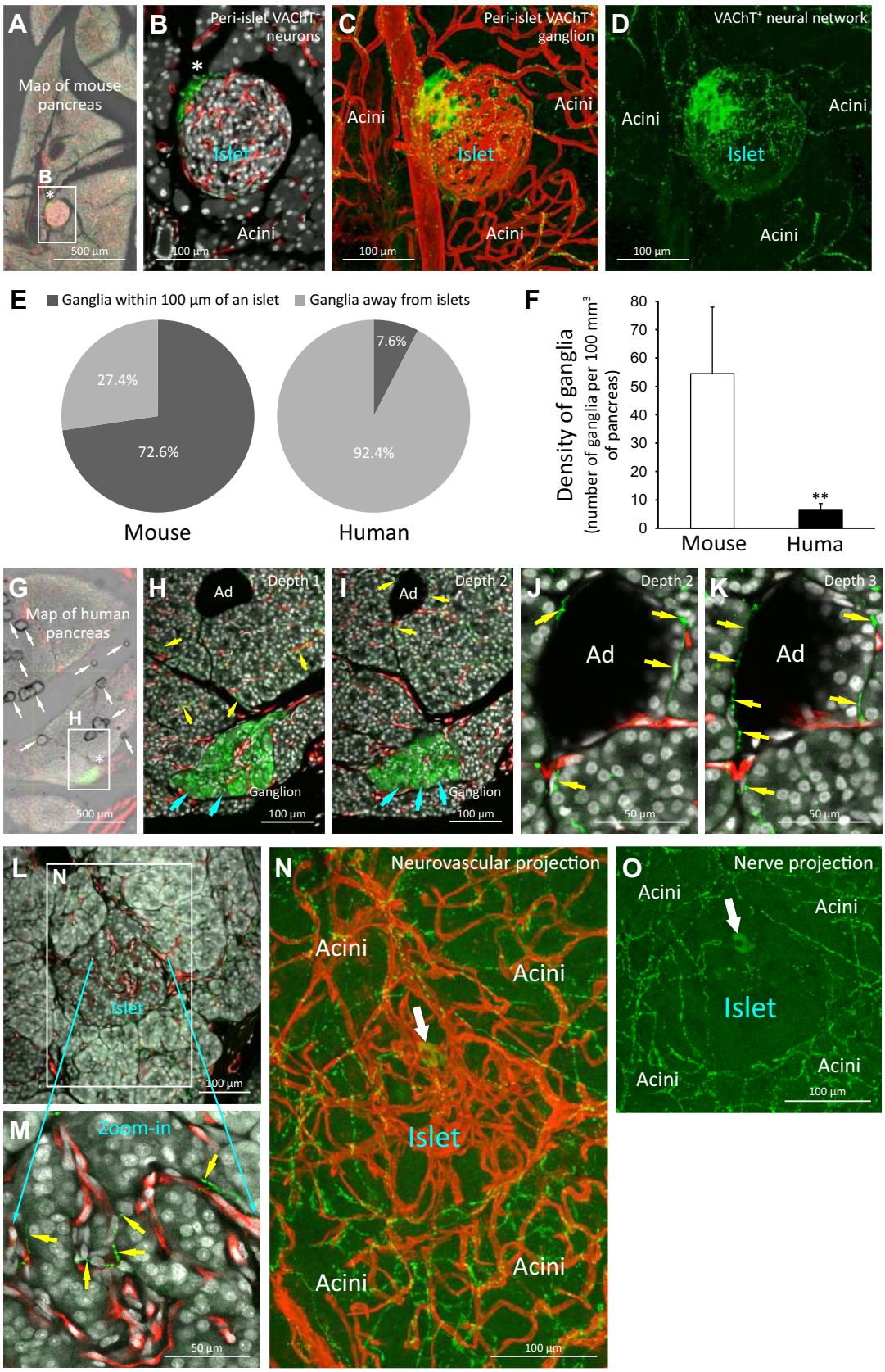

CGRP staining generates poor signal-to-noise ratio, whereas the SP staining reveals the sensory nerves, which are a subset of the overall pancreatic neural network (PGP9.5$^+$, Fig. 2). The SP$^+$ sensory nerves show the following four features in the human pancreas. First, the nerve fibers are sparse, but they can be found at the basal domain of the interlobular ducts (Fig. 2, *A–F*). Second, the SP$^+$ nerves follow the duct to the peri-islet area but do not penetrate into the core (Fig. 2, *D–F* and Supplemental Video S1, http://doi.org/10.5281/zenodo.3373231). Third, the intrapancreatic ganglia are filled with the SP$^+$ varicosities in contact with neurons (Fig. 2, *G–I*). Fourth, the interlobular neural network is partly SP$^+$, which includes a scattered population of SP$^+$ neurons (~7% of neurons in ganglia; Fig. 2, *J–N*).

To confirm the SP-labeled sensory innervation in the disease condition, we apply the same paired staining of SP and PGP9.5 to reveal the sensory nerves and neurons in duct lesion formation (specimens derived from distal pancreatectomy for treatment of patients with ductal adenocarcinoma). Supplemental Figure S1 and Supplemental Video S2 (http://doi.org/10.5281/zenodo.3373231) illustrate the lesion microenvironment and the ganglia in which the immunoreactive SP$^+$ neurons reside.

Similarity and difference between mouse and human pancreatic afferent sensory nerves. Using the same SP staining, in Fig. 3 we present the mouse pancreatic sensory nerves, which is a subset of the PGP9.5-labeled neural network. Similar to their human counterparts, the PGP- and SP-labeled ganglia and the neural network are prominently seen in the mouse pancreas (Fig. 3, *A–F*). In addition, because the mouse pancreatic lobules are relatively small (~500 μm), multiple ganglia, islets, and lobules are simultaneously visualized with panoramic 3-D microscopy (Fig. 3, *A* and *D*). These structures are connected with the PGP9.5$^+$ nerve trunks, which include the SP$^+$ afferent sensory nerves (Fig. 3, *E* and *F*).

The mouse SP$^+$ afferent sensory nerves differ from those in the human pancreas in their islet association (Fig. 3, *G–L* and Supplemental Video S3, http://doi.org/10.5281/zenodo.3373231). In particular, the SP$^+$ nerve fibers and varicosities follow the arteriole to the islet mantle (Fig. 3, *G* and *H*; note that the mouse ganglia often reside around islets, Fig. 3, *K* and *L*) and subsequently extend into the core (Fig. 3*J*). Interestingly, in quantitation, we identify a 124% ($P < 0.001$) higher density of SP$^+$ nerves in the islets than acini (Fig. 3*M*). The difference and the lack of SP$^+$ nerves in the human islets indicate the likely difference(s) in the immunoreactivity of SP and/or the SP$^+$ innervation patterns between the two systems.

Comparison of mouse and human pancreatic efferent parasympathetic nerves. In both mouse and human pancreases, the efferent parasympathetic network, including the intrapancreatic ganglia, can be revealed with VAChT staining (Fig. 4). In mice, the intrapancreatic ganglia often reside around the islets (Fig. 4, *A–E*), and their density is 7.7-fold ($P < 0.01$) higher than their counterparts in humans (Fig. 4*F*). In humans, the intrapancreatic ganglia are sparse and mostly away from the islet (Fig. 4*E*) (i.e., without a nearby landmark for detection). A tissue map is thus needed to first survey the pancreatic lobules (Fig. 4*G*) before zooming in for identification (Fig. 4, *H* and *I*).

One major difference between the adult mouse and human pancreases is the presence of adipocytes inside the lobules (fatty infiltration or steatosis), which is common in the adult humans but not in mice (45, 54, 55, 61). Using the paired transmitted light and fluorescence imaging (Fig. 4, *G–K*), we detect and confirm the parasympathetic innervation of the intralobular adipocytes (VAChT$^+$ fibers and varicosities around adipocytes), implicating that this ectopic fat development is associated with the efferent parasympathetic nerves.

It is worthwhile to note that despite the differences in locations and densities of the mouse and human intrapancreatic ganglia (Fig. 4, *E* and *F*), in both systems their parasympathetic nerve extensions (fibers and varicosities) are seen around the blood vessels. The neurovascular networks travel together, reaching the acinar-islet boundaries and integrating the exocrine and endocrine tissues (Fig. 4, *B–D* and *L–O*). Interestingly, in the magnified images, scattered VAChT$^+$ cells are found in the human islet (Fig. 4, *N* and *O*). Because many neurons and endocrine cells share the ability of amine precursor uptake and decarboxylation (39, 40), the neuronal or endocrine identity of these cells require further investigation.

Comparison of mouse and human pancreatic efferent sympathetic nerves. In both mouse and human pancreases, the efferent sympathetic nerves can be detected with the TH (enzyme of catecholamine synthesis) staining (Fig. 5, *A–F*). Maps of mouse and human pancreases show that the TH$^+$ sympathetic nerves follow the arterioles and capillaries in extension. The perivascular sympathetic nerves associate with the acini and islets in a pattern similar to the parasympathetic innervation. It appears that no TH$^+$ neurons can be seen,

Fig. 4. Comparison of efferent parasympathetic nerves in mouse and human pancreases. *A–D*: vesicular acetylcholine transporter (VAChT)$^+$ ganglion and parasympathetic nerves in mouse pancreas. Gross view in *A* (male, age 12 wk) and zoom-in examination in *B–D* show the islet-ganglionic association. *A* and *B*: * indicates the VAChT$^+$ ganglion. *C* and *D*: signal projections show the connection of VAChT$^+$ varicosities in space and their vascular association. Neurovascular network connects the exocrine (acini) and endocrine (islet) pancreas. Markers: nuclei, white; VAChT, green; blood vessels, red. *E*: evaluation of islet-ganglionic association, mouse vs. human. Fewer ganglia (7.6%) are within 100 μm of an islet in the human pancreas compared with mouse pancreas (72.6%). Sixty-six and 117 ganglia in the human ($n = 4$) and mouse ($n = 6$) pancreases, respectively, were analyzed. Ganglia and islets >50 μm in major axis were used in the analysis. *F*: lower density of intrapancreatic ganglia in humans than in mice. Pancreases from 4 human donors (~400 mm^3 of tissues from each donor) and 6 mice (~70 mm^3 of tissues from each mouse) were used in the analysis; data are presented as means ± SD and analyzed with two-tailed Student's *t* test (**$P < 0.01$). *G–K*: VAChT$^+$ ganglion and adipocyte (Ad) innervation in human pancreas. Gross view in *G* (male, age 53 yr, body mass index 28) and zoom-in examination in *H–K* reveal the VAChT$^+$ intrapancreatic ganglion (*G–I*, green patch) and the parasympathetic nerves around the intralobular adipocyte (*H–K*). *G*: white arrows, adipocytes. *H–K*: yellow arrows, VAChT$^+$ fibers and varicosities. *H* and *I*: cyan arrows, somas of neurons. *L–O*: parasympathetic neurovascular connection of human exocrine and endocrine pancreas. *L* and *M*: VAChT$^+$ parasympathetic nerves (yellow arrows) follow the blood vessels (red, CD31$^+$) from the exocrine domain to the islet core. *N* (*inset* in *L*) and *O*: acinar-islet neurovascular integration. White arrow indicates a VAChT$^+$ cell in the islet.

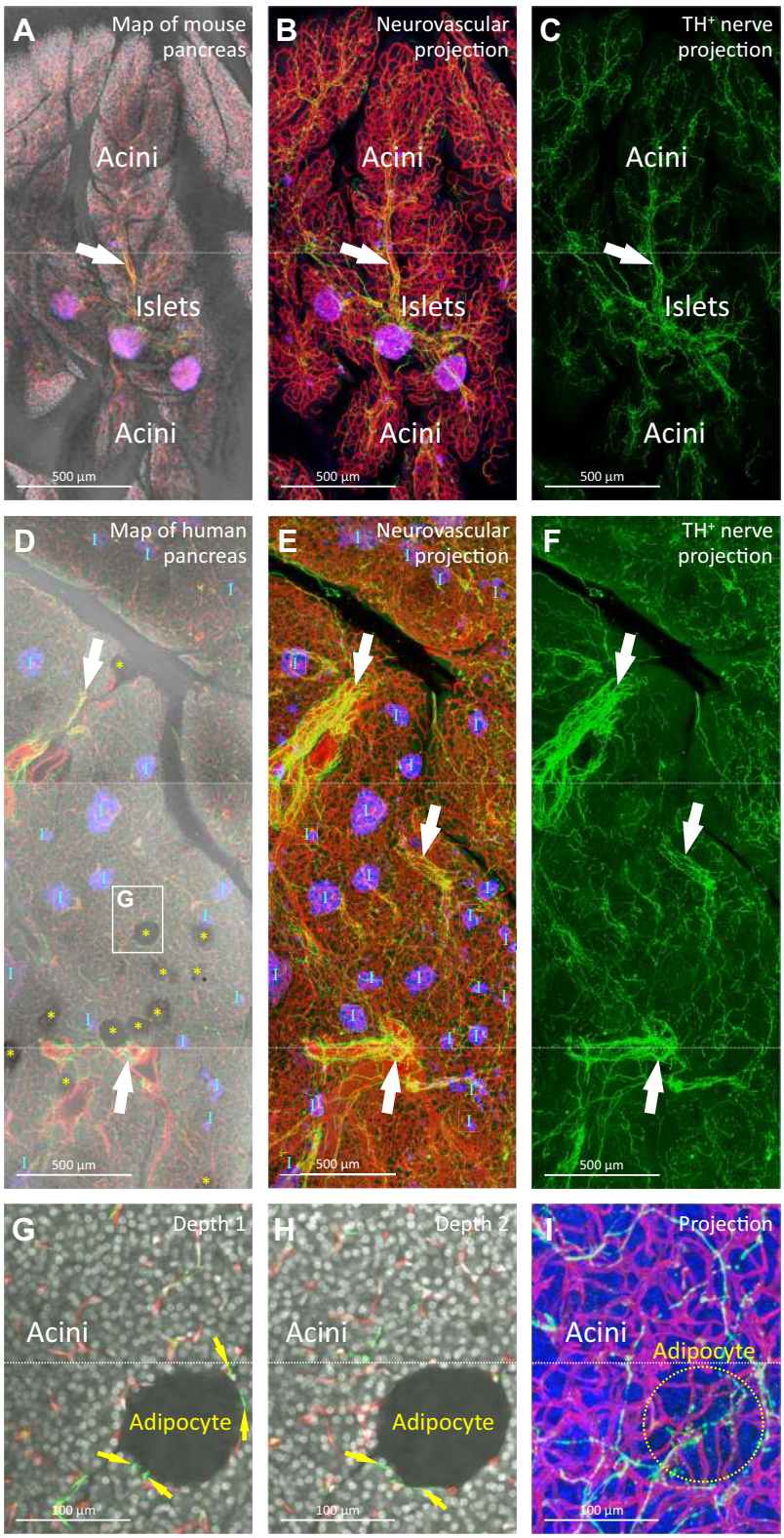

Fig. 5. Comparison of efferent sympathetic nerves in mouse and human pancreases. *A–C*: tyrosine hydroxylase $(TH)^+$ sympathetic nerves in mouse pancreas. Map in *A* (male, age 12 wk) and signal projection in *B* and *C* show the neurovascular association and integration of acini and islets. Arrow indicates the peri-arteriolar sympathetic nerves. *D–F*: human counterparts. Markers: nuclei, white; TH, green; islet (insulin), blue; blood vessels, red. *D–F*: TH^+ sympathetic nerves in human pancreas. Map in *D* (female, age 40 yr, body mass index 24) and signal projection in *E* and *F* show the association of sympathetic nerves with vasculature (arrow, peri-arteriolar nerves). Intralobular adipocytes (asterisk in *D*) are commonly seen in humans but not in mice. Note that the human pancreatic lobule is significantly larger than the mouse counterpart, and the human islets are primarily intralobular. Same markers are used in *A–C* and *D–F*. Letter I, islet. *G–I*: sympathetic innervation of adipocyte. *G* and *H*: focus on the inset in *D* at different focal depths. Both show TH^+ nerves (arrow) contact the adipocyte. *I*: signal projection depicts the nerves extending from the nearby acini to associate with the adipocyte (circle). Markers: nuclei, white/blue; TH, green; CD31 (blood vessels), red.

differing from the SP- and VAChT-labeled pancreases (Figs. 2 and 4), confirming that the sympathetic input to the pancreas is extrinsic.

As demonstrated in Fig. 4, *G–K*, one major difference between the mouse and human pancreases is the frequent presence of intralobular adipocytes in the pancreas. These adipocytes contact not only the pancreatic subunits (acini and islets), but also the efferent parasympathetic (Fig. 4, *G–K*) and sympathetic nerves (Fig. 5, *G–I*); the latter features TH^+ axons and varicosities in the immediate microenvironment of adi-

pocytes. The results reveal that both arms of the efferent nerves could influence the adipocyte physiology.

Ganglionic colocalization of afferent and efferent nerves in health and duct lesion formation. In the human intrapancreatic ganglia, the concentrated SP^+ (Fig. 2*M*) and $VAChT^+$ (Fig. 4*H*) signals strongly suggest that the sensory and parasympathetic nerves associate with each other at this location. Using the quadruple staining of PGP9.5, SP, VAChT, and nuclei, we confirm that the SP^+ and $VAChT^+$ neurons colocalize in the ganglia (Fig. 6, *A* and *B*), and the efferent $VAChT^+$ neurons

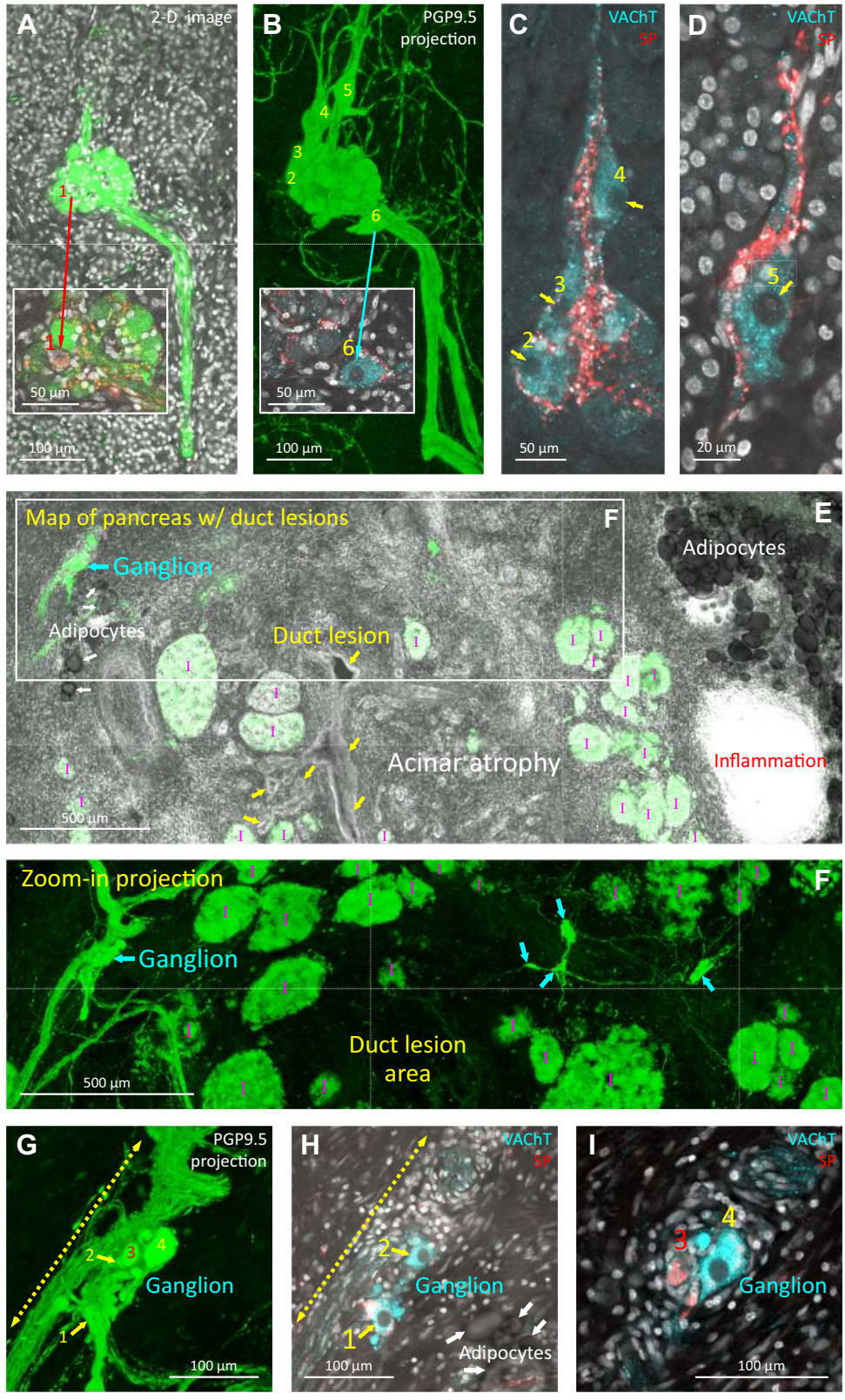

Fig. 6. Afferent and efferent nerve association in health and duct lesion formation. *A* and *B*: Co-localization of substance P $(SP)^+$ and vesicular acetylcholine transporter $(VAChT)^+$ neurons in human intrapancreatic ganglion. *A–D*: 6 neurons (no. 1–6; female, age 51 yr, body mass index 20) are presented. *Insets*: SP^+ (*A*, red; no. 1) and $VAChT^+$ (*B*, cyan; no. 6) neurons (arrows). *A* and *B* examine the same ganglion. Markers: PGP9.5, green; SP, red; VAChT, cyan; nuclei, white. *C* and *D*: neurons no. 2–5 are presented. These neurons are $VAChT^+$ and surrounded by SP^+ varicosities. *C*: contacts/overlaps of SP^+ (red) and $VAChT^+$ (cyan) signals appear as white dots around the neurons. Arrows in *C* and *D* indicate the dimly stained nuclei. *E* and *F*: pancreatic innervation and intrapancreatic ganglia in duct lesion formation. *E*: an area 5 cm distal to the pancreatic ductal adenocarcinoma (male, age 52 yr, staging T2N0). Yellow arrows indicate the duct lesions. In the peri-lesional microenvironment, four features are typically seen: acinar atrophy, islet aggregation (letter I, islet), inflammation, and adipocyte infiltration. Ganglia (cyan arrows in *E* and *F*) are found around the lesion and associated with the infiltrated adipocytes (top left; enlarged in *G–I*). *G–I*: colocalization of ganglionic SP^+ and $VAChT^+$ neurons in duct lesion formation. Dashed arrow, nerve bundle. Four neurons (no. 1–4) are presented. No. 1, 2, and 4: $VAChT^+$ neurons. No. 3: SP^+ neuron. *H*: adipose-ganglionic association. White arrows: adipocytes.

are surrounded by the SP^+ varicosities (Fig. 6, *C* and *D*). The result provides the histological evidence of a potential afferent-efferent reflex pathway in the human pancreas.

To explore this afferent-efferent neuronal association in the disease condition, the same quadruple staining is used to investigate the pancreatic innervation in duct lesion formation (Fig. 6, *E–I*). The tissue map (Fig. 6*E*) depicts an area 5 cm distal to the pancreatic ductal adenocarcinoma with apparent acinar atrophy, inflammation, and adipocyte infiltration. The intralobular adipocytes are used as the landmark to locate the ganglion (Fig. 6, *E* and *H*). This is based on the known tendency of the adipose-ganglionic association in the human pancreas (55). Importantly, the enlarged images of the ganglion confirm that, despite the loss of parenchyma (acinar atrophy), the SP^+ and $VAChT^+$ neurons still reside in the remodeled pancreas and associate with each other (Fig. 6, *F–I*). The result highlights the intrinsic pancreatic neurons and their continuous presence in the deformed pancreas in duct lesion progression.

DISCUSSION

Because of the technical challenges in specimen preparation and deep-tissue imaging, the human pancreatic afferent and efferent nerves have not been globally examined to illustrate the exocrine, endocrine, and adipose innervation in an integrated fashion. In this research, we prepare transparent pancreases for 3-D neurohistology, which avoids the potential false-negative and false-positive interferences in fluorescent imaging (Fig. 1). Using the multidimensional and multiplex signals, we simultaneously illustrate the pancreatic microstructures (including the ectopic adipocytes) and neurovascular networks in space, which otherwise cannot be easily defined via the standard microtome-based two-dimensional histology.

Our 3-D image data show that the human pancreatic neural network consists of the afferent SP^+ sensory nerves, the efferent $VAChT^+$ parasympathetic and TH^+ sympathetic nerves, and the intrapancreatic ganglia with SP^+ (scattered minority, ~7%) and $VAChT^+$ neurons. The SP^+ afferent nerves associate with the interlobular ducts (Fig. 2), whereas the $VAChT^+$ and TH^+ efferent nerves reside at the peri-acinar and perivascular spaces. Both the parasympathetic and sympathetic nerves form the neurovascular networks that bridge the exocrine (acini) and endocrine (islets) pancreas (Figs. 4 and 5). Compared with the mouse pancreas, the human pancreas differs in *1*) the lack of intra-islet SP^+ afferent nerves (Fig. 2, *D–F* vs. Fig. 3, *G–J*), *2*) the lower ganglionic density (Fig. 4*F*), and *3*) the obvious presence of $VAChT^+$ parasympathetic and TH^+ sympathetic nerves around the intralobular adipocytes (Fig. 4, *G–K* and Fig. 5, *G–I*). Table 1 summarizes the innervation patterns revealed in the human and mouse pancreatic tissues.

The ectopic fat accumulation in the pancreas has been suggested to affect the pancreatic exocrine and endocrine functions (47, 60). The accumulation occurs as early as the teenage years and the degree is linked with obesity (25). In the adipose innervation, although the sympathetic innervation of fat pads (brown and white) has been well established (6, 7), it remains controversial regarding the fat pad-specific parasympathetic innervation (20, 26). Whereas the sympathetic inputs contribute to lipolysis, the parasympathetic influences have been implicated for modulation of the insulin-mediated glucose uptake by adipocytes (26, 35). In Fig. 4, *G–K* and Fig. 5, *G–I*, we confirm that the ectopic fat in the human pancreatic lobules is associated with the parasympathetic as well as sympathetic nerves, implicating that both arms of the efferent nerves can influence the pancreatic adipocyte population. This is similar to the finding of Kreier et al. (26) of both sympathetic and parasympathetic innervation of the intra-abdominal and subcutaneous white adipose tissues in rats. Interestingly, because the high insulin concentrations in the pancreas promote adipogenesis (48), the insulin stimulation and the parasympathetic input could act in concert in causing fat accumulation as observed in the adult human pancreas in health and type 2 diabetes (19, 26, 55). However, it should be noted that the anatomic data presented in Fig. 4, *G–K* and Fig. 5, *G–I* require additional functional studies to fully establish the parasympathetic and sympathetic influences on the ectopic fat accumulation in the pancreas.

In the studies of pancreatic innervation and of pain in pancreatitis and pancreatic cancer, SP staining has been routinely used to reveal the pancreatic sensory nerves and their potential activation (10, 29, 43, 44, 46, 62). However, to the best of our knowledge, the immunoreactive SP^+ neurons in the human pancreas, as presented in Figs. 2 and 6 and Supplemental Fig. S1 and Supplemental Video S1 (http://doi.org/10.5281/zenodo.3373231), have not been described. In the gut, it has been known that the intrinsic afferent neurons have their cell bodies and processes within the intestine, which directly or indirectly associate with the epithelium for monitoring the gut lumen activities and reflex activation (17, 18). Similar to the enteric neural pathway, in the pancreas the ganglionic afferent (immunoreactive SP) and efferent (immunoreactive VAChT) association suggests that the pancreatic sensory information may not be totally conveyed to the central nervous system. Instead, a local reflex pathway may directly respond to the sensory nerve activation, monitoring the epithelial microenvironment. On the basis of this anatomic evidence, future re-

Table 1. *Summary of pancreatic innervation patterns revealed in humans and mice*

	Afferent Nerves, Sensory (Immunoreactive SP)		Efferent Nerves, Parasympathetic (Immunoreactive VAChT)		Efferent Nerves, Sympathetic (Immunoreactive TH)	
	Human*	Mouse	Human*	Mouse	Human	Mouse
Exocrine gland	√	√	√	√	√	√
Endocrine gland	N.F.	√	√	√	√	√
Ectopic fat	N.A.	N.A.	√	N.A.	√	(56)†

√, identified in this research; N.A., not analyzed in this research; N.F., not found in this research; SP, substance P; TH, tyrosine hydroxylase; VAChT, vesicular acetylcholine transporter. *Examined in both normal pancreases from cadaveric donors and surgical biopsies distal to the tumor bulk of pancreatic ductal adenocarcinoma; †Identified in reference 56.

search should focus on establishing the synaptic connections between the sensory and parasympathetic neurons in the intrapancreatic ganglia, confirming the reflex center in the human pancreas.

Anatomically, unlike the enteric ganglia with known locations (submucosal and myenteric plexuses), the human intrapancreatic ganglia are scattered inside and around the lobules without a known pattern and in a low density (Fig. 4*F*). This uncertainty, therefore, demands tissue mapping to survey the area of interest (e.g., Fig. 2*A*, Fig. 4*G*, and Fig. 6*E*) and then zoom in to confirm the neuronal association. In this research, we use panoramic and 3-D histology with tissue clearing to facilitate tissue mapping and characterization of the intrapancreatic ganglia. However, our optical approach is limited by two factors. First, the tissue clearing-based microscopy is not compatible with functional imaging because of the unphysiological osmotic pressure of the clearing reagent (53). Second, we only indirectly see the nerves through immunolabeling (SP, VAChT, or TH staining), which may not reflect the overall neural networks in the pancreas. For example, we suspect that the SP staining only reveals a subset of the sensory nerves that use the neuropeptide in communication rather than the entire sensory network. Nevertheless, our imaging approach provides a strategy to systematically detect and characterize the neural network, including the intrapancreatic ganglia, in health (Fig. 6, *A–D*) and duct lesion formation (Fig. 6, *E–I*). In particular, the latter features tissue remodeling with inflammation, adipocyte infiltration, and acinar atrophy, indicating that the image analysis is not limited to the normal human pancreas.

In summary, using the multidimensional and multiplex optical signals, we identify and characterize the human pancreatic afferent and efferent innervation patterns and the intrapancreatic ganglia. Our work builds the technical and anatomical foundations for future detailed neurohistological analyses of the human pancreas in health and disease.

ACKNOWLEDGMENTS

The authors are grateful for the support from the confocal imaging core in National Tsing Hua University, which is sponsored by the Ministry of Science and Technology, Taiwan (MOST 104–2731-M-007–002).

GRANTS

This work was supported in part by grants from Taiwan Academia Sinica (AS-107-TP-L15) to Y.-W. Tien and S.-C. Tang, Ministry of Science and Technology (MOST 106-2321-B-002 −034) to Y.-W. Tien, and Taiwan National Health Research Institutes (NHRI EX107-10524EI) and MOST (106-2314-B-007-004-MY2 and 108-2314-B-007-006-MY2) to S.-C. Tang.

DISCLOSURES

No conflicts of interest, financial or otherwise, are declared by the authors.

AUTHOR CONTRIBUTIONS

H.-J.C., T.-C.C., S.-J.P., M.-H.C., Y.-H.C., C.-Y.L., Y.-M.J., Y.-W.T., and S.-C.T. conceived and designed research; H.-J.C., T.-C.C., S.-J.P., M.-H.C., Y.-H.C., C.-Y.L., Y.-M.J., and Y.-W.T. performed experiments; H.-J.C., T.-C.C., S.-J.P., M.-H.C., Y.-H.C., C.-Y.L., Y.-M.J., Y.-W.T., and S.-C.T. analyzed data; H.-J.C., T.-C.C., S.-J.P., M.-H.C., Y.-H.C., C.-Y.L., Y.-M.J., Y.-W.T., and S.-C.T. interpreted results of experiments; H.-J.C., T.-C.C., S.-J.P., and S.-C.T. prepared figures; Y.-W.T. and S.-C.T. drafted manuscript; H.-J.C., T.-C.C., S.-J.P., M.-H.C., Y.-H.C., C.-Y.L., Y.-M.J., Y.-W.T., and S.-C.T. edited and revised manuscript; H.-J.C., T.-C.C., S.-J.P., M.-H.C., Y.-H.C., C.-Y.L., Y.-M.J., Y.-W.T., and S.-C.T. approved final version of manuscript.

REFERENCES

1. **Ahrén B.** Autonomic regulation of islet hormone secretion—implications for health and disease. *Diabetologia* 43: 393–410, 2000. doi:10.1007/s001250051322.
2. **Ahrén B, Holst JJ.** The cephalic insulin response to meal ingestion in humans is dependent on both cholinergic and noncholinergic mechanisms and is important for postprandial glycemia. *Diabetes* 50: 1030–1038, 2001. doi:10.2337/diabetes.50.5.1030.
3. **Arvidsson U, Riedl M, Elde R, Meister B.** Vesicular acetylcholine transporter (VAChT) protein: a novel and unique marker for cholinergic neurons in the central and peripheral nervous systems. *J Comp Neurol* 378: 454–467, 1997. doi:10.1002/(SICI)1096-9861(19970224)378:4<454:AID-CNE2>3.0.CO;2-1.
4. **Babic T, Browning KN, Kawaguchi Y, Tang X, Travagli RA.** Pancreatic insulin and exocrine secretion are under the modulatory control of distinct subpopulations of vagal motoneurones in the rat. *J Physiol* 590: 3611–3622, 2012. doi:10.1113/jphysiol.2012.234955.
5. **Barreto SG, Carati CJ, Toouli J, Saccone GT.** The islet-acinar axis of the pancreas: more than just insulin. *Am J Physiol Gastrointest Liver Physiol* 299: G10–G22, 2010. doi:10.1152/ajpgi.00077.2010.
6. **Bartness TJ, Liu Y, Shrestha YB, Ryu V.** Neural innervation of white adipose tissue and the control of lipolysis. *Front Neuroendocrinol* 35: 473–493, 2014. doi:10.1016/j.yfrne.2014.04.001.
7. **Bartness TJ, Vaughan CH, Song CK.** Sympathetic and sensory innervation of brown adipose tissue. *Int J Obes* 34, *Suppl* 1: S36–S42, 2010. doi:10.1038/ijo.2010.182.
8. **Begg DP, Woods SC.** Interactions between the central nervous system and pancreatic islet secretions: a historical perspective. *Adv Physiol Educ* 37: 53–60, 2013. doi:10.1152/advan.00167.2012.
9. **Bou Karam J, Cai W, Mohamed R, Huang T, Meng L, Homan EP, Dirice E, Kahn CR, El Ouaamari A.** TRPV1 neurons regulate β-cell function in a sex-dependent manner. *Mol Metab* 18: 60–67, 2018. doi:10.1016/j.molmet.2018.10.002.
10. **Büchler M, Weihe E, Fries H, Malfertheiner P, Bockman E, Müller S, Nohr D, Beger HG.** Changes in peptidergic innervation in chronic pancreatitis. *Pancreas* 7: 183–192, 1992. doi:10.1097/00006676-199203000-00009.
11. **Ceyhan GO, Bergmann F, Kadihasanoglu M, Altintas B, Demir IE, Hinz U, Müller MW, Giese T, Büchler MW, Giese NA, Friess H.** Pancreatic neuropathy and neuropathic pain--a comprehensive pathomorphological study of 546 cases. *Gastroenterology* 136: 177–186.e1, 2009. doi:10.1053/j.gastro.2008.09.029.
12. **Chien HJ, Peng SJ, Hua TE, Kuo CH, Juang JH, Tang SC.** 3-D imaging of islets in obesity: formation of the islet-duct complex and neurovascular remodeling in young hyperphagic mice. *Int J Obes* 40: 685–697, 2016. doi:10.1038/ijo.2015.224.
13. **Demir IE, Friess H, Ceyhan GO.** Neural plasticity in pancreatitis and pancreatic cancer. *Nat Rev Gastroenterol Hepatol* 12: 649–659, 2015. doi:10.1038/nrgastro.2015.166.
14. **Franco-Cereceda A, Henke H, Lundberg JM, Petermann JB, Hökfelt T, Fischer JA.** Calcitonin gene-related peptide (CGRP) in capsaicin-sensitive substance P-immunoreactive sensory neurons in animals and man: distribution and release by capsaicin. *Peptides* 8: 399–410, 1987. doi:10.1016/0196-9781(87)90117-3.
15. **Fu YY, Lin CW, Enikolopov G, Sibley E, Chiang AS, Tang SC.** Microtome-free 3-dimensional confocal imaging method for visualization of mouse intestine with subcellular-level resolution. *Gastroenterology* 137: 453–465, 2009. doi:10.1053/j.gastro.2009.05.008.
16. **Fu YY, Peng SJ, Lin HY, Pasricha PJ, Tang SC.** 3-D imaging and illustration of mouse intestinal neurovascular complex. *Am J Physiol Gastrointest Liver Physiol* 304: G1–G11, 2013. doi:10.1152/ajpgi.00209.2012.
17. **Furness JB.** The enteric nervous system and neurogastroenterology. *Nat Rev Gastroenterol Hepatol* 9: 286–294, 2012. doi:10.1038/nrgastro.2012.32.
18. **Furness JB.** Novel gut afferents: intrinsic afferent neurons and intestinofugal neurons. *Auton Neurosci* 125: 81–85, 2006. doi:10.1016/j.autneu.2006.01.007.
19. **Géloën A, Collet AJ, Guay G, Bukowiecki LJ.** Insulin stimulates in vivo cell proliferation in white adipose tissue. *Am J Physiol Cell Physiol* 256: C190–C196, 1989. doi:10.1152/ajpcell.1989.256.1.C190.

20. **Giordano A, Song CK, Bowers RR, Ehlen JC, Frontini A, Cinti S, Bartness TJ.** White adipose tissue lacks significant vagal innervation and immunohistochemical evidence of parasympathetic innervation. *Am J Physiol Regul Integr Comp Physiol* 291: R1243–R1255, 2006. doi:10.1152/ajpregu.00679.2005.
21. **Gregg BE, Moore PC, Demozay D, Hall BA, Li M, Husain A, Wright AJ, Atkinson MA, Rhodes CJ.** Formation of a human β-cell population within pancreatic islets is set early in life. *J Clin Endocrinol Metab* 97: 3197–3206, 2012. doi:10.1210/jc.2012-1206.
22. **Human Cell Atlas Organizing Committee.** *The Human Cell Atlas White Paper*. https://arxiv.org/abs/1810.05192, 2018.
23. **Juang JH, Peng SJ, Kuo CH, Tang SC.** Three-dimensional islet graft histology: panoramic imaging of neural plasticity in sympathetic reinnervation of transplanted islets under the kidney capsule. *Am J Physiol Endocrinol Metab* 306: E559–E570, 2014. doi:10.1152/ajpendo.00515.2013.
24. **Kent C, Clarke PJ.** The immunolocalisation of the neuroendocrine specific protein PGP9.5 during neurogenesis in the rat. *Brain Res Dev Brain Res* 58: 147–150, 1991. doi:10.1016/0165-3806(91)90248-H.
25. **Kovanlikaya A, Mittelman SD, Ward A, Geffner ME, Dorey F, Gilsanz V.** Obesity and fat quantification in lean tissues using three-point Dixon MR imaging. *Pediatr Radiol* 35: 601–607, 2005. doi:10.1007/s00247-005-1413-y.
26. **Kreier F, Fliers E, Voshol PJ, Van Eden CG, Havekes LM, Kalsbeek A, Van Heijningen CL, Sluiter AA, Mettenleiter TC, Romijn JA, Sauerwein HP, Buijs RM.** Selective parasympathetic innervation of subcutaneous and intra-abdominal fat--functional implications. *J Clin Invest* 110: 1243–1250, 2002. doi:10.1172/JCI0215736.
27. **Leahy JL, Fineman MS.** Impaired phasic insulin and amylin secretion in diabetic rats. *Am J Physiol Endocrinol Physiol* 275: E457–E462, 1998. doi:10.1152/ajpendo.1998.275.3.E457.
28. **Lin PY, Peng SJ, Shen CN, Pasricha PJ, Tang SC.** PanIN-associated pericyte, glial, and islet remodeling in mice revealed by 3D pancreatic duct lesion histology. *Am J Physiol Gastrointest Liver Physiol* 311: G412–G422, 2016. doi:10.1152/ajpgi.00071.2016.
29. **Liu L, Shenoy M, Pasricha PJ.** Substance P and calcitonin gene related peptide mediate pain in chronic pancreatitis and their expression is driven by nerve growth factor. *JOP* 12: 389–394, 2011.
30. **Liu YA, Chen Y, Chiang AS, Peng SJ, Pasricha PJ, Tang SC.** Optical clearing improves the imaging depth and signal-to-noise ratio for digital analysis and three-dimensional projection of the human enteric nervous system. *Neurogastroenterol Motil* 23: e446–e457, 2011. doi:10.1111/j.1365-2982.2011.01773.x.
31. **Liu YA, Chung YC, Pan ST, Hou YC, Peng SJ, Pasricha PJ, Tang SC.** 3-D illustration of network orientations of interstitial cells of Cajal subgroups in human colon as revealed by deep-tissue imaging with optical clearing. *Am J Physiol Gastrointest Liver Physiol* 302: G1099–G1110, 2012. doi:10.1152/ajpgi.00432.2011.
32. **Love JA, Yi E, Smith TG.** Autonomic pathways regulating pancreatic exocrine secretion. *Auton Neurosci* 133: 19–34, 2007. doi:10.1016/j.autneu.2006.10.001.
33. **Maggi CA.** Principles of tachykininergic co-transmission in the peripheral and enteric nervous system. *Regul Pept* 93: 53–64, 2000. doi:10.1016/S0167-0115(00)00177-4.
34. **McCrimmon RJ, Sherwin RS.** Hypoglycemia in type 1 diabetes. *Diabetes* 59: 2333–2339, 2010. doi:10.2337/db10-0103.
35. **Messina G, Valenzano A, Moscatelli F, Salerno M, Lonigro A, Esposito T, Monda V, Corso G, Messina A, Viggiano A, Triggiani AI, Chieffi S, Guglielmi G, Monda M, Cibelli G.** Role of autonomic nervous system and orexinergic system on adipose tissue. *Front Physiol* 8: 137, 2017. doi:10.3389/fphys.2017.00137.
36. **Mundinger TO, Mei Q, Figlewicz DP, Lernmark A, Taborsky GJ Jr.** Impaired glucagon response to sympathetic nerve stimulation in the BB diabetic rat: effect of early sympathetic islet neuropathy. *Am J Physiol Endocrinol Metab* 285: E1047–E1054, 2003. doi:10.1152/ajpendo.00136.2003.
37. **Mussa BM, Verberne AJ.** The dorsal motor nucleus of the vagus and regulation of pancreatic secretory function. *Exp Physiol* 98: 25–37, 2013. doi:10.1113/expphysiol.2012.066472.
38. **O'Connor TM, O'Connell J, O'Brien DI, Goode T, Bredin CP, Shanahan F.** The role of substance P in inflammatory disease. *J Cell Physiol* 201: 167–180, 2004. doi:10.1002/jcp.20061.
39. **Ohta Y, Kosaka Y, Kishimoto N, Wang J, Smith SB, Honig G, Kim H, Gasa RM, Neubauer N, Liou A, Tecott LH, Deneris ES, German MS.** Convergence of the insulin and serotonin programs in the pancreatic β-cell. *Diabetes* 60: 3208–3216, 2011. doi:10.2337/db10-1192.
40. **Pearse AG.** The diffuse neuroendocrine system: peptides, amines, placodes and the APUD theory. *Prog Brain Res* 68: 25–31, 1986. doi:10.1016/S0079-6123(08)60229-0.
41. **Rodriguez-Diaz R, Abdulreda MH, Formoso AL, Gans I, Ricordi C, Berggren PO, Caicedo A.** Innervation patterns of autonomic axons in the human endocrine pancreas. *Cell Metab* 14: 45–54, 2011. doi:10.1016/j.cmet.2011.05.008.
42. **Secchi A, Caldara R, Caumo A, Monti LD, Bonfatti D, Di Carlo V, Pozza G.** Cephalic-phase insulin and glucagon release in normal subjects and in patients receiving pancreas transplantation. *Metabolism* 44: 1153–1158, 1995. doi:10.1016/0026-0495(95)90008-X.
43. **Sharkey KA, Williams RG, Dockray GJ.** Sensory substance P innervation of the stomach and pancreas. Demonstration of capsaicin-sensitive sensory neurons in the rat by combined immunohistochemistry and retrograde tracing. *Gastroenterology* 87: 914–921, 1984. doi:10.1016/0016-5085(84)90088-X.
44. **Shen Q, Wang Y, Zhang N, Gao D, Liu Y, Sha L.** Substance P expresses in intrapancreatic ganglia of the rats. *Neuropeptides* 59: 33–38, 2016. doi:10.1016/j.npep.2016.06.004.
45. **Singh RG, Yoon HD, Wu LM, Lu J, Plank LD, Petrov MS.** Ectopic fat accumulation in the pancreas and its clinical relevance: A systematic review, meta-analysis, and meta-regression. *Metabolism* 69: 1–13, 2017. doi:10.1016/j.metabol.2016.12.012.
46. **Sinha S, Fu YY, Grimont A, Ketcham M, Lafaro K, Saglimbeni JA, Askan G, Bailey JM, Melchor JP, Zhong Y, Joo MG, Grbovic-Huezo O, Yang IH, Basturk O, Baker L, Park Y, Kurtz RC, Tuveson D, Leach SD, Pasricha PJ.** PanIN neuroendocrine cells promote tumorigenesis via neuronal cross-talk. *Cancer Res* 77: 1868–1879, 2017. doi:10.1158/0008-5472.CAN-16-0899.
47. **Smits MM, van Geenen EJ.** The clinical significance of pancreatic steatosis. *Nat Rev Gastroenterol Hepatol* 8: 169–177, 2011. doi:10.1038/nrgastro.2011.4.
48. **Sorisky A.** From preadipocyte to adipocyte: differentiation-directed signals of insulin from the cell surface to the nucleus. *Crit Rev Clin Lab Sci* 36: 1–34, 1999. doi:10.1080/10408369991239169.
49. **Stagner J, Ahren B, Sundler F, White K.** Reconstructing the pancreas: restoration of normoglycemia, exocrine function, and islet innervation by islet transplantation to the pancreas. *Transplant Proc* 40: 452–454, 2008. doi:10.1016/j.transproceed.2008.01.031.
50. **Taborsky GJ Jr.** Islets have a lot of nerve! Or do they? *Cell Metab* 14: 5–6, 2011. doi:10.1016/j.cmet.2011.06.004.
51. **Taborsky GJ Jr, Mei Q, Hackney DJ, Figlewicz DP, LeBoeuf R, Mundinger TO.** Loss of islet sympathetic nerves and impairment of glucagon secretion in the NOD mouse: relationship to invasive insulitis. *Diabetologia* 52: 2602–2611, 2009. doi:10.1007/s00125-009-1494-5.
52. **Taborsky GJ Jr, Mundinger TO.** Minireview: the role of the autonomic nervous system in mediating the glucagon response to hypoglycemia. *Endocrinology* 153: 1055–1062, 2012. doi:10.1210/en.2011-2040.
53. **Tainaka K, Kuno A, Kubota SI, Murakami T, Ueda HR.** Chemical principles in tissue clearing and staining protocols for whole-body cell profiling. *Annu Rev Cell Dev Biol* 32: 713–741, 2016. doi:10.1146/annurev-cellbio-111315-125001.
54. **Takahashi M, Hori M, Ishigamori R, Mutoh M, Imai T, Nakagama H.** Fatty pancreas: A possible risk factor for pancreatic cancer in animals and humans. *Cancer Sci* 109: 3013–3023, 2018. doi:10.1111/cas.13766.
55. **Tang SC, Baeyens L, Shen CN, Peng SJ, Chien HJ, Scheel DW, Chamberlain CE, German MS.** Human pancreatic neuro-insular network in health and fatty infiltration. *Diabetologia* 61: 168–181, 2018. doi:10.1007/s00125-017-4409-x.
56. **Tang SC, Shen CN, Lin PY, Peng SJ, Chien HJ, Chou YH, Chamberlain CE, Pasricha PJ.** Pancreatic neuro-insular network in young mice revealed by 3D panoramic histology. *Diabetologia* 61: 158–167, 2018. doi:10.1007/s00125-017-4408-y.
57. **Teff KL.** Cephalic phase pancreatic polypeptide responses to liquid and solid stimuli in humans. *Physiol Behav* 99: 317–323, 2010. doi:10.1016/j.physbeh.2009.11.009.

58. **Teff KL.** How neural mediation of anticipatory and compensatory insulin release helps us tolerate food. *Physiol Behav* 103: 44–50, 2011. doi:10.1016/j.physbeh.2011.01.012.
59. **Travagli RA, Browning KN.** Central autonomic control of the pancreas. In: *Central Regulation of Autonomic Functions*, edited by Llewellyn-Smith I and Verberne AJ. New York: Oxford University Press, 2011, p. 274–291.
60. **van Herpen NA, Schrauwen-Hinderling VB.** Lipid accumulation in non-adipose tissue and lipotoxicity. *Physiol Behav* 94: 231–241, 2008. doi:10.1016/j.physbeh.2007.11.049.
61. **Wang CY, Ou HY, Chen MF, Chang TC, Chang CJ.** Enigmatic ectopic fat: prevalence of nonalcoholic fatty pancreas disease and its associated factors in a Chinese population. *J Am Heart Assoc* 3: e000297, 2014. doi:10.1161/JAHA.113.000297.
62. **Won MH, Park HS, Jeong YG, Park HJ.** Afferent innervation of the rat pancreas: retrograde tracing and immunohistochemistry in the dorsal root ganglia. *Pancreas* 16: 80–87, 1998. doi:10.1097/00006676-199801000-00013.
63. **Yosten GLC.** Alpha cell dysfunction in type 1 diabetes. *Peptides* 100: 54–60, 2018. doi:10.1016/j.peptides.2017.12.001.